TiO_2 Nanotube / Chalcogenide-based Photo-electrochemical Cell: Nanotube Diameter Dependence Study

Miloš Krbal[1], Hanna Sopha[1], Veronika Podzemná[1], Sayantan Das[1], Jan Prikryl, Jan M. Macak[1*]

[1]Center of Materials and Nanotechnologies, Faculty of Chemical Technology, University of Pardubice, Nam. Cs. Legii 565, 53002 Pardubice, Czech Republic

* Corresponding author: e-mail jan.macak@upce.cz

Abstract: We present photo-electrochemical results for anodic TiO_2 nanotube layers grown with different diameter sizes (21, 35, 56 and 95 nm) with a thickness of approx. 560 nm using a novel anodization protocol. These tube layers were utilized as highly ordered n-type conductive scaffold for the inorganic chromophore Sn-S-Se. While downscaling the nanotube diameter significantly increased the number of nanotubes per square unit (from 5.6E+09 to 7.2E+10 pcs/cm^2) and thus the active surface area increased as well, we found that the photo-electrochemical response in the UV light was identical and thus independent of the TiO_2 nanotube diameter in the range of nanotube diameters from 35 to 95 nm. Further, we demonstrate that a heterostructured photo-electrochemical cell consisting of TiO_2 nanotubes sensitized with crystalline Sn-S-Se chromophore showed higher photocurrent density (from 6 to 32 µA/cm^2 for the wavelength of 460 nm) with increasing nanotube diameter size. Upon detailed SEM analyses it was revealed that the Sn-S-Se was infilled in all nanotube layers approximately to one third of the thickness. Therefore, this photocurrent increase with increasing tube diameter can be ascribed to better interfacial contact (and improved charge transport) facilitated between the chromophore and nanotube walls.

1. Introduction

Today, there is a clear worldwide consensus regarding the need for the long-term replacement of fossil fuels by low-cost, high-efficient, renewable and environmentally friendly sources of energy. Photovoltaic technologies encounter a tremendous development to meet this target. While the single crystal silicon solar cells possess high efficiency ~25 %[1], the initial cost and their fragility motivated researchers to focus on new type thin film-based devices, such as amorphous silicon[2], CdTe[3] or $CuGa_{1-x}In_xSe_2$ (CIGS)[4], dye-sensitized cells[5], organic cells[6] and perovskite solar cells[7] that can be deposited on various substrates. However, these technologies are not as efficient on the large scale, though they possess distinct advantages compared to silicon solar cells, such as transparency and flexibility, low cost fabrication and better performance under diffuse sun illumination.

Further, it was shown that controlling the TiO_2 - chromophore interface increases the efficiency of the cells[5, 7]. Such enhancement can be achieved by increasing the interfacial surface

area between the chromophore and the TiO_2 in order to facilitate efficient charge separation. Unlike mesoporous TiO_2 supports, ordered nanostructures, such as high aspect ratio self-organized TiO_2 nanotube layers[8-10] or epitaxially grown TiO_2 nanorods[11, 12], offer the advantage of directed charge transport and controlled phase separation between donor and acceptor parts of the solar cell and thus they seem very promising for nanoscale solar hybrid technologies[9].

Recently, non-silicon solar cells based on TiO_2 nanotube layers sensitized by organic dyes[8], perovskites[13] and chalcogenides[14-17] have been presented. The latter class of materials is comparably more stable under UV light and ambient conditions, which make these materials promising for future generation of solar cell devices. As in the case of organic dyes or organohalide perovskites, the absorbing chalcogenide layer can be deposited via a solvent solution process, i.e. a hydrazine-based[18-20] or a mixture of 1,2-ethylenediamine + 1,2-ethanedithiol-based[21] solutions. This process is amenable to infill or coat TiO_2 nanotube layers in order to form hybrid solar cells easily and cheaply. To the best of the author´s knowledge, there is no report on the sensitization of TiO_2 nanotube layers by crystalline chromophores using spincoating.

For instance, $Cu_2ZnSn(Se,S)_4$ (CZTSSe) in its kesterite phase[22, 23] has recently emerged as an attractive candidate in thin film solar cells, as it has similar properties as $CuIn_xGa_{(1-x)}(S,Se)_2$ (CIGSSe) cells but with the rare and/or expensive In and Ga being replaced with the earth abundant and less expensive Zn and Sn. While CZTSSe can be deposited by the solution process, the hydrazine-based solution contains $ZnSe(N_2H_4)$ crystals with a crystal size of approx. 100 nm[24]. This discriminates the applicability of CZTSSe as a chromophore within here presented experiments due to narrower nanotube diameters. Since the main goal was to investigate the photoresponse of TiO_2 nanotube layers with different diameters infilled with an inorganic chromophore on chalcogenide basis, one could consider a less absorbing chromophore in the far visible spectral range beyond a wavelength of ~650 nm. However, the chromophore should follow these criteria: (i) have good solubility in NH_2-based solvent, (ii) be in a nanocolloidal solution and (iii) possess high charge mobility. Based on the literature and our experiences, binary or ternary systems of Sn[18, 23, 24] or Sb[21, 25] based chalcogenide could be the best possible choice. Experimentally, it was found that Sn-chalcogenides were better soluble than Sb-chalcogenides, especially in propylamine, and thus Sn-S-Se was singled out as the ideal chromophore for further photo-electrochemical studies.

Herein, we present at first a novel anodization protocol and photo-electrochemical response for anodic TiO_2 nanotube layers grown with different diameters (between approx. 21 and 95 nm) with a constant thickness of approx. 560 nm. At second, we demonstrate photo-electrochemical and structural characterization of the heterostructured photo-chemical half-cells, fabricated using highly ordered n-type conductive TiO_2 nanotubular scaffolds infilled by spin-coating with an inorganic crystalline chromophore Sn-S-Se dissolved in propylamine solvent.

2. Experimental Section

2.1. Growth of TiO_2 nanotube layers with different diameters

Prior to anodization the Ti substrates (Sigma-Aldrich, 0.127 mm, 99.7 % purity) were degreased by sonication in isopropanol and acetone, then rinsed with isopropanol and dried in air. The electrochemical setup consisted of a 2 electrode configuration using a platinum foil as the counter electrode, while the Ti substrates (working electrodes) were pressed against an O-ring of

the electrochemical cell, leaving 1 cm^2 open to the electrolyte. Electrochemical experiments were carried out at room temperature employing a high-voltage potentiostat (PGU-200V, IPS Elektroniklabor GmbH).

A glycerol based electrolyte was used containing 0.27 M NH_4F and 50 vol.% H_2O. All electrolytes were prepared from reagent grade chemicals. The Ti foils were anodized were anodized at 7, 10, 15 and 25 V with a sweep rate of 1 V/s for different times, i.e. 180 min, 70 min or 20 min, in order to obtain TiO_2 nanotubes with different diameters (21, 35, 56 and 95 nm) and at the same time to preserve the nanotube layer thickness which is ~560 nm. Note, in the case of TiO_2 nanotubes with the diameter of 21 nm, the maximum nanotube layer thickness reached 370 nm, which was the experimental limit under these growing conditions. After anodization, the Ti substrates were rinsed and sonicated in isopropanol and dried in air. In order to convert amorphous nanotube layers to anatase nanotube layers, annealing at 400 °C for 1 h in air with a heating and cooling rate of 2 °C/min was carried out in a muffle oven.

The nanotube dimensions and related parameters corresponding to anodization conditions are summarized in Tab. 1. Figure S1 shows also individual histograms used for the evaluation of nanotube diameters.

Table 1. Growth conditions, inner diameter (D) and thickness statistics (l) of TiO_2 nanotube layers of TiO_2 per cm^2, number of nanotubes per cm^2 (N) and estimated surface area of nanotubes per 1 cm^2 of nanotube layer (A).

Sample	**21 nm**	**35 nm**	**56 nm**	**95 nm**
U (V)	7	10	15	25
t (min)	180	180	70	20
D (nm)	21.4 ± 3.1	35.6 ± 5.6	56.4 ± 8.8	94.7 ± 14.3
l (µm)	0.37 ± 0.03	0.56 ± 0.07	0.53 ± 0.06	0.57 ± 0.02
N (pcs/cm^2)	7.2E+10	2.6E+10	1E+10	5.6E+09
A (cm^2)	56.1	48.5	26.5	24.1

2.2. Heterostructured systems of TiO_2 nanotube layers coated by crystalline Sn-S-Se from solvent solutions

The $SnSe_2$ bulk crystalline sample was synthesized using the standard melt-quench technique. Pure elements of 5N purity were precisely weighed and placed in pre-cleaned silica ampoules. The ampoules were evacuated at a pressure of 1×10^{-3} Pa for 30 min and then sealed.

The syntheses were performed in a rocking furnace with ampoules exposed to a temperature of 1000 °C for 24 h and subsequently quenched into cold water to avoid any phase segregation**.**
The chalcogenide solution was prepared following the procedure reported by Mitzi et al.[18], except that the hydrazine was replaced by propylamine. 0.5 g $SnSe_2$ were placed into a 10 ml volumetric flask and then mixed with 5 ml of propylamine. Further, a single droplet of hydrazine was necessary to inject into the system in order to initiate the dissolution process. During dissolution a total amount of 0.1 g of S was added to dissolve $SnSe_2$ completely and thus to obtain a homogeneous solution. Heterostructures of TiO_2 nanotube layers infilled by crystalline Sn-S-Se were prepared via the spin-coating technique. 100 µl of the solution were dropped on TiO_2 nanotube layers covering an area of 1 cm^2 and spread out homogeneously by spinning with the spin speed of 2000 rpm for 30 s. Next, the as-prepared heterostructures were annealed at 125 °C or 200 °C for 10 h under vacuum with a residual pressure of 5 Pa to remove the organic solvent and/or the excess of chalcogens.

The structure and morphology of the TiO_2 nanotube layers and prepared heterostructures were characterized by a field-emission SEM (FE SEM JEOL JSM 7500F). Dimensions of the nanotubes were measured and statistically evaluated using proprietary Nanomeasure software. For each condition used in this work, average values and standard deviations were calculated from at least 3 different locations on 2 samples of each condition, with a high number of measurements ($n \geq 100$). The crystallinity of deposited Sn-S-Se thin films was measured using the Advance D8 Bruker X-ray diffractometer set to Cu-K line. The composition of Sn-S-Se samples spin-coated on the top of TiO_2 nanotube layers and annealed at 125 and 200°C was measured by EDX.

In order to obtain information about the photo-electrochemical properties of the nanotube layers and the heterostructured systems of TiO_2 nanotube layers infilled by Sn-S-Se, photocurrent measurements were carried out in an aqueous electrolyte containing 0.1 M Na_2SO_4, employing a photoelectric spectrophotometer (Instytut Fotonowy), connected with the modular electrochemical system PGSTAT 204 (Metrohm Autolab B.V.), and operated with *Nova 1.10* software. A three-electrode cell with a flat quartz window was employed with an Ag/AgCl reference electrode, a Pt wire counter electrode, and Ti substrate with anodic nanotube layers as working electrode, pressed against an O-ring of the electrochemical cell leading to an irradiated sample area of 0.28 cm^2. Monochromatic light was provided by a 150 W Xe lamp. The photocurrents were measured at a constant potential of 0.7 V vs. Ag/AgCl in the spectral range from 300 to 800 nm. A shutter of the monochromator was opened for 10 s to obtain a stable plateau of the photocurrent values. The IPCE value for for each wavelength was calculated according to the equation $IPCE\ (\%) = (i_{ph}hc)/(\lambda Pq)x100$, where i_{ph} is the photocurrent density, h is Planck's constant, c is velocity of light, P is the light power density, λ is the irradiation wavelength and q is the elementary charge.

3. Results and Discussion

3.1. TiO_2 nanotube layers with different diameters

Figure 1 shows SEM images of the self-organized TiO_2 nanotube layers used in this work. The inspection of SEM images disclosed that all nanotube layer surfaces were clean and without obvious surface defects (missing nanotubes, cracks, etc.). The inner diameters and the thicknesses of the nanotube layers (see Tab. 1) were evaluated by statistical analyses of the SEM images from the top views (Fig. 1), and from the cross-sections of the nanotube layers. The SEM images were

also used to estimate the number of nanotubes per cm^2 and the corresponding active surface area. All aforementioned parameters are summarized in Tab. 1. As one can see, the down-scaling of the nanotube diameter towards significantly lower diameters (lower than common among TiO_2 nanotube layers published) leads to an increase of the number of nanotubes per square unit. Thus the active surface area of the whole layer increases as well.

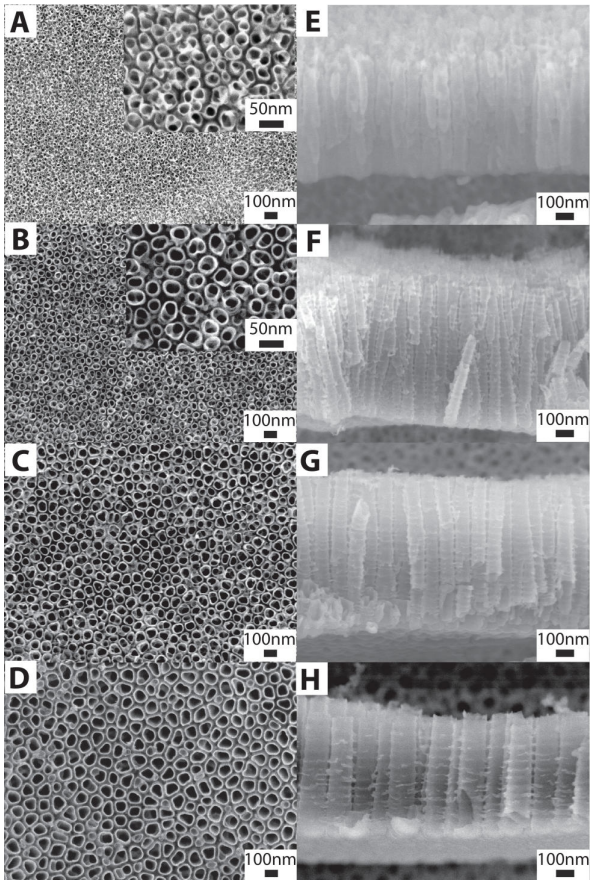

Figure 1. SEM top-view images of self-organized TiO_2 nanotube layers with different average nanotube diameters: A) 21 nm, B) 35 nm, C) 56 nm and D) 95 nm. SEM images E-H represent cross-sections of corresponding TiO_2 nanotube layers. Insets in A) and B) show layers at higher magnification.

It was assumed that the significant increase of the number of nanotubes per cm^2 may have the potential to enhance the photocurrent response of heterostructured solar cells due to the increase of the interfacial surface area between the chromophore and the TiO_2 nanotube layers. To address this expectation, we probed as the first step the role of the active surface area size of the plane anodic TiO_2 nanotube layers shown in Fig. 1 on electronic properties via the photo-electrochemical experiments. However, one can see from Fig. 2 that photocurrent densities and IPCE values were similar, reaching maximum values of 16 $\mu A/cm^2$ at 340 nm and 55 % at 330 nm, respectively. It turned out that the photon-to-electron conversion was independent of the TiO_2 nanotube diameter in the range of nanotube diameters from 35 to 95 nm. These are interesting results, and to the best of authors shown for the first time for nanotube layers.

However, they are not surprising due to the fact that the electron diffusion length for these relatively thin layers (approx. 560 nm) is larger than the light absorption depth, as described in previous literature independently by Lindquist et al. and Peter [26, 27]. In other words, for nanotube layers with the same thickness, the photocurrent density generated upon UV illumination is approximately the same, regardless the tube diameter. Photocurrent densities are in this case limited by the speed of recombination of charge carriers [28], which does not depend on surface of the nanotubes, but rather their length (translated into the nanotube layer thickness). The reason for the remaining nanotube layers (with an average diameter of 21 nm) to exhibit lower photocurrent densities (about 36 % lower values) is that they are about 34 % thinner (~370 nm) than the others. Since the decrease in photocurrent density corresponds well with the decrease in the layer thickness, one can come to the conclusion that the light, passing through the thinner nanotube layer, was not sufficiently absorbed to achieve an efficient light harvesting in the UV light spectral range [29].

Further, one can see from Fig. 2C that the photocurrent raised immediately when the nanotube layers were exposed to the UV light. Similarly, when the UV light was cut off, a sharp de-excitation was observed. This means that the charges generated near the top of the nanotube layers did not suffer from the series of trapping-detrapping processes that slowed down the charge motion upon travelling across the entire nanotube layer thickness.

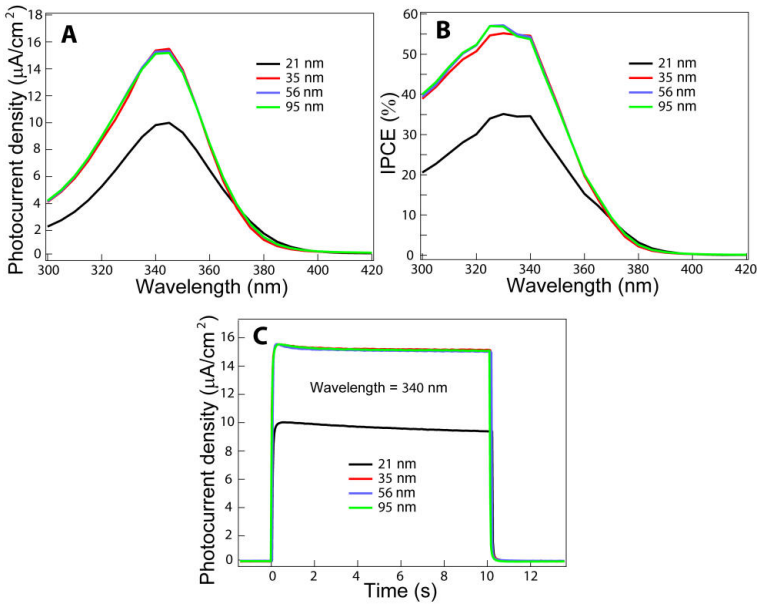

Figure 2. A) photocurrent density B) incident photon-to-electron conversion efficiency and C) photocurrent transients recorded for ~560 nm thick anatase TiO_2 nanotube layers with different diameters.

3.2. Heterostructured photo-chemical half-cells of TiO_2 nanotube layers coated by crystalline Sn-S-Se

In the second step, we tested the set of self-organized TiO_2 nanotube layers shown in Fig. 1 as host scaffolds for potential heterostructured solar cell devices. In general, there are a few ways, how to achieve efficient light harvesting of TiO_2 layers in the visible spectral range by suitable chromophores[5, 7, 30]: bath deposition, spin-coating, electrodeposition, or atomic layer deposition. In this work we employed spin-coating for an infiltration of crystalline chalcogenide chromophore (Sn-S-Se) within the TiO_2 nanotube layers, as recently reported in literature for amorphous chalcogenide[14]. Since the diameter of nanotubes was scaled down to 21 nm, special requirements on chalcogenides were necessary for infilling such very fine porous scaffold as described in introduction part (solvent selection, etc.).

In order to demonstrate the level of Sn-S-Se infilling within the TiO_2 nanotube layers with different diameter, we carried out extensive SEM cross-sectional analyses of infilled nanotube layers. Figure 3 shows comparison of SEM images taken from the Sn-S-Se infilled TiO_2 nanotube layers with an average nanotube diameter of 35 nm. It can be seen are infilled with the Sn-S-Se material from approximately one third of the nanotube layer thickness. This level is approximately the same for all other nanotube layers with different diameters. Figure S2 provides additional SEM images to evidence the infilling.

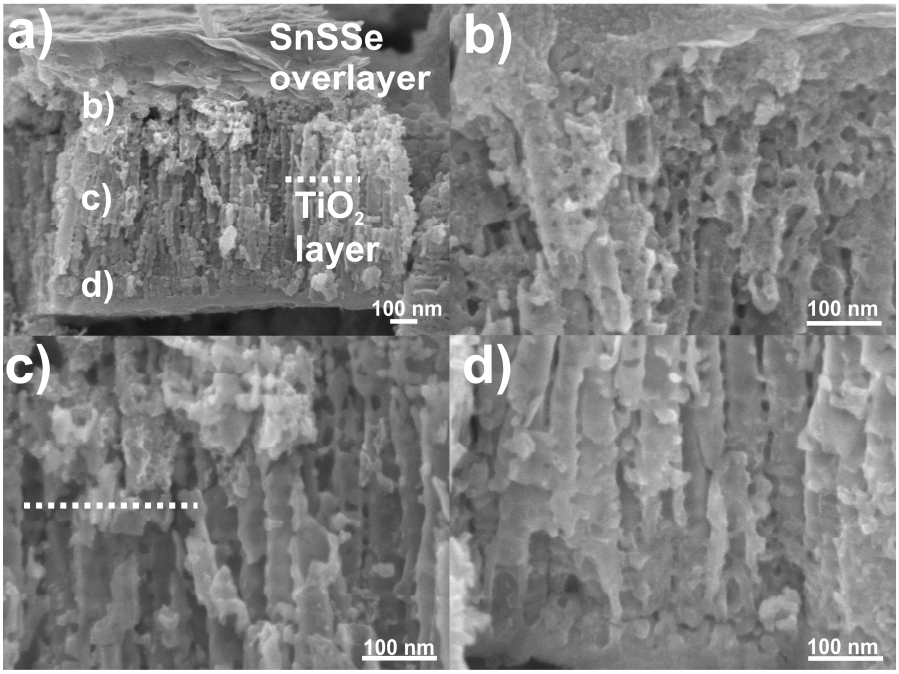

Figure 3. Cross-sectional SEM images of the Sn-S-Se infilled TiO_2 nanotube layers with nanotube diameter of 35 nm: A) the main cross-section of the whole layer indicating locations of where higher magnification images at three different nanotube layer depths shown in B)-D) we taken. The dotted lines represent the approximate depth of Sn-S-Se infilling within the nanotube layer (Sn-S-Se material can be found in approximately one third of the nanotube layer thickness).

When TiO_2 nanotube layers were infilled with crystalline Sn-S-Se, a significant photocurrent response in the visible spectral range was observed, as shown in Fig. 4A, reaching the maximum at 465 nm. It can be also seen from Fig. 4A that the photocurrent density in VIS was similar for nanotube layers with inner diameter 95 and 56 nm and gradually decreased for nanotube layers with inner diameter 35 and 21 nm. In other words, the photocurrent response was enhanced by a factor of six from nanotube layers with diameter 21 nm to 56 (95) nm. However, these results were not obtained due to different infilling level, as discussed in Fig. 3.

Looking at Fig. 4B, the IPCE values achieved 8 % in maximum at 465 nm which is not the best possible result. It has to be pointed out that the total thickness of spin-coated chalcogenide chromophore layer on TiO_2 nanotube layer was only about 300 nm (confirmed by SEM from the cross-sectional view – see Fig. 4C, regardless of the tube diameter) in comparison with the CZTSSe-based solar cells having the thickness ~2 μm[20]. Therefore the present IPCE values are lowered due to insufficient light absorption. Further, Sn-S-Se deposited on the top of TiO_2 nanotube layers absorbs a part of the UV light which originally interacted with TiO_2 nanotube layers and thus the IPCE value in the UV region drops from 40% (blank sample) to 16% (sensitized sample).

Since the infilling degree of Sn-S-Se within TiO_2 nanotube layers is approximately same, as discussed in Fig. 3, it is likely the contact of Sn-S-Se within TiO_2 nanotube layers that plays the major role on the photon-to-electron conversion and differences seen in Fig. 4A-B. Using field-emission SEM, we investigated the quality of the Sn-S-Se layer on the top of nanotube layers and we found that the film consists of three different layers as can be seen in Fig. 4C-F. Going from the top, the first layer was formed with a compact nanocrystalline layer with the thickness ~100 nm (marked as “top layer” in Fig. 4C). The second layer consisted of randomly oriented Sn-S-Se discs with rounded hexagonal shape and average size of 150 nm in diameter and 20 nm thick (see Fig. 4C and D) located on the nanotube openings. The total thickness of the second layer was about 200 nm. Finally, the third layer was directly embedded (infilled) within the nanotube layers and formed the nanotube – chalcogenide interface. It is evident from Fig. 4E and F that the growth of an mesoporous chalcogenide layer following (elongating) the TiO_2 nanotube layer scaffolds seems to have discontinuous Sn-S-Se network on TiO_2 nanotubes with 21 nm in diameter, whereas it shows continuous network on TiO_2 nanotubes with 95 nm in diameter. One can suppose that this continuous mesoporous chalcogenide layer might be responsible for better charge transport from chalcogenide-to-TiO_2 nanotube layers and thus enhance the photocurrent results of heterostructured devices based on TiO_2 nanotube layers with 56 and 95 nm in diameter utilized as chromophore scaffolds.

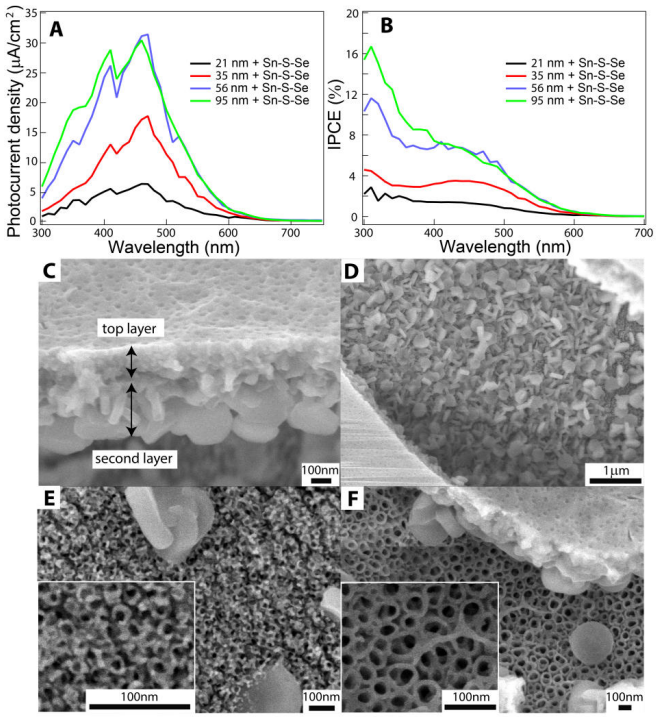

Figure 4. A) photocurrent density B) incident photon-to-electron conversion efficiency of anatase TiO_2 nanotube layers with different diameters sensitized with crystalline Sn-S-Se films deposited by spin-coating. C) to F) represent SEM images of: C) a cross-section of an intentionally peeled off Sn-S-Se film which was deposited by spin-coating on the top of the TiO_2 nanotube layer with the nanotube diameter of 21 nm after annealing at 125 °C , D) randomly oriented Sn-S-Se discs with rounded hexagonal shape and average size of 150 nm in diameter and 20 nm thick that are underneath the top layer, E) and F) the growth of a mesoporous chalcogenide layer elongating within the TiO_2 nanotubes with 21 nm and 95 nm in diameter, respectively. This mesoporous layer is located underneath layers described in C) and D).

Additionally, the IPCE values presented here were also affected by tuning of the chromophore composition by annealing conditions[18, 31]. Recently, we have reported that the optimal annealing protocol for low-aspect ratio TiO_2 nanotube layers is 400 °C for 1 h in order to obtain the best photo-electrochemical response[32]. It is known from the literature that the best performance of chalcogenide-based solar cell devices is achieved when annealed over 500 °C. However, to prevent modification of TiO_2 nanotubular scaffolds infilled with the Sn-S-Se chromophore by approaching or exceeding 400 °C, two temperature steps, i.e. 125 °C and 200 °C for 10 h under a residual pressure of 5 Pa were selected in our experiments. One can see from Fig. 5A and B an approx. 50 % improvement of the photo-electrochemical response of the heterostructured device exposed to 200 °C compared to 125 °C. In addition, the spectral range of absorption was broadened to 800 nm due to the change in band gap from 1.9 to 1.42 eV (see Fig. 5C), as a consequence of the shift in the composition from $Sn_{33}S_{25}Se_{42}$ (a presence of a small amount of O in layers was observed) to $Sn_{33.5}S_{33.5}Se_{33.5}$ (probed by EDX). It is fair to note that a possible additional release of the remnant organic solvent at 200 °C may also contribute to the decrease in band gap. The compositional change of the film upon annealing was also well

observed from the Bragg diffractions (see Fig. 5D). SnS_xSe_{2-X} crystallizes in a CdI_2 – like layered hexagonal structure (P-3m1)[33, 34]. From the XRD spectra, one can see that (001) is the most intensive diffraction peak which indicates on the preferential growth of SnS_xSe_{2-X} and also one can see the shift to higher 2 theta upon annealing at 200 °C that corresponds to the formation of the $Sn_{33.5}S_{33.5}Se_{33.5}$ hexagonal phase. These results clearly show that annealing at higher temperature was beneficial for a better performance due to the compositional arrangement along with releasing of the organic solvent.

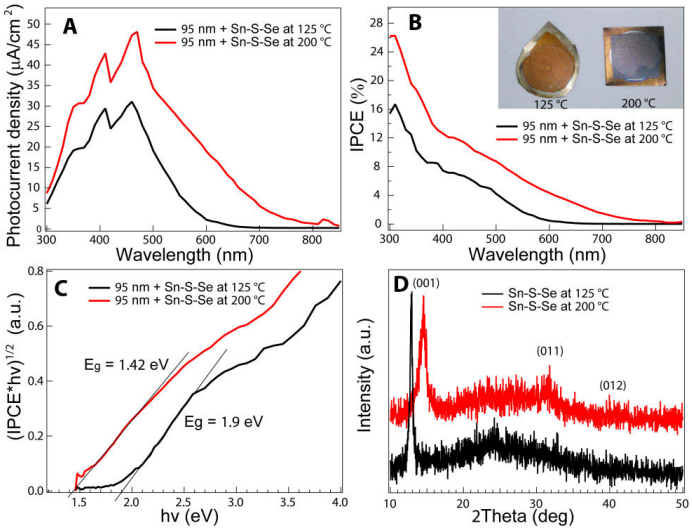

Figure 5. A) photocurrent density B) incident photon-to-electron conversion efficiency recorded for ~560 nm thick anatase TiO_2 nanotube layers with the nanotube diameter ~95 nm diameter, infilled by crystalline Sn-S-Se and annealed at 125 °C and 200 °C, C) estimation of optical band gaps and D) Bragg diffraction of crystalline Sn-S-Se annealed at 125 °C and 200 °C. Inset in B) shows photographs of corresponding samples.

Finally, we have constructed a simplified potential diagram of Ti/TiO_2/Sn-S-Se interface at pH 7 (see Fig. 6). The position of the band edges of Sn-S-Se annealed at 125 °C (green) and 200 °C (red) was determined by assuming that the position of the Fermi level was pinned in the middle of the band gap in analogy to crystalline Sn-S[35]. The photocurrent onset of TiO_2/Sn-S-Se was experimentally determined from CV curves to be *ca.* -0.48 and -0.55 V *vs.* NHE for Sn-S-Se annealed at 125 °C and 200 °C, respectively under 480 nm.

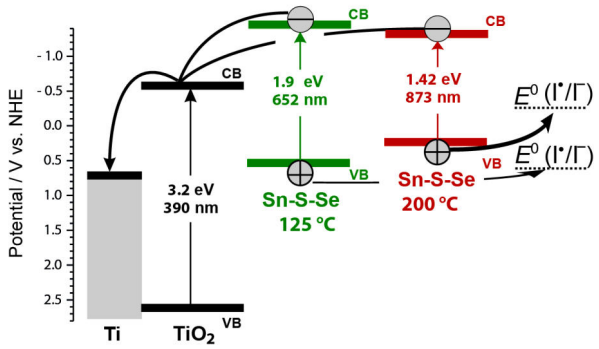

Figure 6. Simplified potential diagram of the Ti/TiO_2/Sn-S-Se interface at pH=7 vs. NHE. The position of the band edges of Sn-S-Se annealed at 125 °C (green) and 200 °C (red) was determined by assuming that the position of the Fermi level was in the middle of the band gap at *ca.* -0.48 and -0.55 V *vs.* NHE, respectively; the band edge positions of TiO_2 were taken from the literature [36].

4. Conclusions

We presented novel anodization protocol and photo-electrochemical results for anodic TiO_2 nanotubes grown with different diameter sizes (21, 35, 56 and 95 nm) utilized as highly ordered n-type conductive scaffold for inorganic chromophore (Sn-S-Se). While downscaling the nanotube diameter significantly increased the number of nanotubes per square unit and thus the active surface area increased as well, we found that the photo-electrochemical response was identical and thus independent of the TiO_2 diameter nanotube size, but it correlated with the thickness of the nanotube layers. Further, we demonstrated that a heterostructured photo-electrochemical cell consisting of TiO_2 nanotubes sensitized with crystalline Sn-S-Se showed higher photocurrent density with increasing nanotube diameter size. The larger openings of the nanotubes may facilitate the penetration of the chromophore deeper into the nanotube layers and therefore enhance the charge transfer from the chromophore to the TiO_2 nanotube layers.

Acknowledgments

European Research Council and Ministry of Youth, Education and Sports of the Czech Republic are acknowledged for financial support of this work through projects 638857 and LM2015082, respectively. We thank to assoc. prof. Ludvik Benes and Mr. Stanislav Slang for XRD and EDX measurements, respectively.

Supporting Information.

Histograms of inner nanotube diameters of TiO_2 nanotube layers; cross-sectional SEM images of the Sn-S-Se infilled TiO_2 nanotube layers; diffuse reflectance spectra of the Sn-S-Se films.

References

(1) Green, M. A.; Emery, K.; Hishikawa, Y.; Warta, W.; Dunlop, E. D. Solar cell efficiency tables (version 48). *Progress in Photovoltaics: Research and Applications*, **2016**, *24*, 905-913.

(2) Carlson; D. E.; Wronski, C. R. Amorphous silicon solar cell. *Appl. Phys. Lett.*, **1976**, *28*, 671.

(3) Britt, J.; Ferekides, C. Thin-film CdS/CdTe solar cell with 15.8% efficiency. *Appl. Phys. Lett.*, **1993**, *62*, 2851.

(4) Jackson, P; Hariskos, D.; Lotter, E.; Paetel, S.; Wuerz, R.; Menner, R.; Wischmann, W.; Powalla, M. New world record efficiency for Cu(In,Ga)Se_2 thin-film solar cells beyond 20%. *Progress in Photovoltaics: Research and Applications*, **2011**, *19*, 894-897.

(5) O´Regan, B.; Grätzel, M. A low-cost, high-efficiency solar cell based on dye-sensitized colloidal TiO_2 films. *Nature*, **1991**, *353*, 737-740.

(6) Wohrle, D.; Meissner, D. Organic solar cells. *Adv. Mat.*, **1991**, *3***,** 129-138.

(7) Liu, M; Johnston, M. M.; Snaith, H. J. Efficient planar heterojunction perovskite solar cells by vapour deposition. *Nature*, **2013**, *501*, 395-398.

(8) So, S.; Hwang, I.; Schmuki, P. Hierarchical DSSC structures based on “single walled” TiO_2 nanotube arrays reach a back-side illumination solar light conversion efficiency of 8%. *Energy and Environ. Sci.*, **2015**, *8*, 849-854.

(9) Mirabolghasemi, H; Liu, N.; Lee, K.; Schmuki, P. Formation of 'single walled' TiO_2 nanotubes with significantly enhanced electronic properties for higher efficiency dye-sensitized solar cells. *Chem. Commun.*, **2013**, *49*, 2067-2069.

(10) Macak, J. M.; Tsuchiya, H.; Ghicov, A.; Yasuda, K.; Hahn, R.; Bauer, S.; Schmuki, P. TiO_2 nanotubes: Self-organized electrochemical formation, properties and applications. *Curr. Opin. Solid State Mater. Sci.* **2007**, *11*, 3–18.

(11) Kim, W. S.; Jang, Y. G.; Kim, D. H. ; Kim, H. C.; Hong, S. H. Hetero-epitaxial growth of vertically-aligned TiO_2 nanorods on an *m*-cut sapphire substrate with an (001) SnO_2 buffer layer *CrystEngComm***,** **2012**,*14*, 4963-4966.

(12) Kim, H. S.; Lee, J. W.; Yantara, N.; Boix, P. P.; Kulkarni, S. A.; Mhaisalkar, S.; Grätzel, M. ; Park, N. G. High efficiency solid-state sensitized solar cell-based on submicrometer rutile TiO_2 nanorod and $CH_3NH_3PbI_3$ perovskite sensitizer *Nano Lett.*, **2013**, *13*, 2412-2417.

(13) Gao, X.; Li, J.; Baker, J.; Hou, Y.; Guan, D.; Chen, J.; Yuan, C. Enhanced photovoltaic performance of perovskite $CH_3NH_3PbI_3$ solar cells with freestanding TiO_2 nanotube array films *Chem. Commun*, **2014**, *50*, 6368-6371.

(14) Macak, J. M.; Kohoutek, T.; Wang, L.; Beranek, R. Fast and robust infiltration of functional material inside titania nanotube layers: case study of a chalcogenide glass sensitizer. *Nanoscale*, **2013**, *5*, 9541-9545.

(15) Mukherjee, B.; Wilson, W; Subramanian, V. S. TiO_2 nanotube (T_NT) surface treatment revisited: Implications of ZnO, $TiCl_4$, and H_2O_2 treatment on the photoelectrochemical properties of T_NT and T_NT–CdSe. *Nanoscale*, **2013**, *5*, 269-274.

(16) Fernandes, J. A.; Migowski, P.; Fabrim,Z.; Feil,A. F.; Rosa, G.; Khan,S.; Machado, G. J.; Fichtner, P. F.P.; Teixeira,S. R.; Santos, M. J. L. et al., J. TiO_2 nanotubes sensitized with CdSe via RF magnetron sputtering for photoelectrochemical applications under visible light irradiation *Phys.Chem.Chem.Phys.*, **2014**, *16*, 9148-9153.

(17) Samu,G. F.; Csaba Visy, C.; Rajeshwar, K.; Sarker, S.; Subramanian, V. R.; Janáky, C. Photoelectrochemical infiltration of a conducting polymer (PEDOT) into metal-chalcogenide decorated TiO_2 nanotube arrays. *Electrochimica Acta*, **2015**, *151*, 467-476.

(18) Mitzi, D. B.; Kosbar, L. L.; Murray, C. E.; Copel, M.; Afzali, A. High-mobility ultrathin semiconducting films prepared by spin coating. *Nature*, **2004**, *428*, 299-303.

(19) Todorov, T. K.; Gunawan, O.; Gokmen, T.; Mitzi, D. B. Solution-processed $Cu(In,Ga)(S,Se)_2$ absorber yielding a 15.2% efficient solar cell *Prog. Photovolt: Res. Appl.* **2013**, *21*, 82-87.

(20) Todorov, T. K.; Tang, J.; Bag, S.; Gunawan, O.; Gokmen, T.; Zhu, Y.; Mitzi, D. B. Beyond 11% efficiency: characteristics of state-of-the-art $Cu_2ZnSn(S,Se)_4$ solar cells. *Adv. Energy Mater*., **2013**, *3*, 34-38.

(21) Webber, D. H.; Brutchey, R. L. Alkahest for V_2VI_3 chalcogenides: Dissolution of nine bulk semiconductors in a diamine-dithiol solvent mixture. *J. Am. Chem. Soc.*, **2013**, *135*, 15722-15725.

(22) Katagiri, H.; Sasaguchi, N.; Hando, S.; Hoshino, S.; Ohashi, J.; Yokota, T. Preparation and evaluation of Cu_2ZnSnS_4 thin films by sulfurization of E-B evaporated precursors. *Sol. Energy Mater.* Sol. Cells **1997**, *49*, 407-414.

(23) Yang, W.; Duan, H. S.; Bob, B.; Zhou, H.; Lei, B.; Chung, C. H.; Li, S. H.; Hou, W. W.; Yang, Y. Novel solution processing of high-efficiency earth-abundant $Cu_2ZnSn(S,Se)_4$ solar cells. *Adv. Mater*. **2012**, *24*, 6323-6329.

(24) Todorov, T. K.; Reuter, K. B.; Mitzi, D. B. High-efficiency solar cell with earth-abundant liquid-processed absorber. *Adv. Mater*. **2010**, *22*, E156-E159.

(25) Zhou, Y.; Leng, M.; Xia, Z.; Zhong, J.; Song, H.; Liu, X.; Yang, B.; Zhang, J.; Chen, J.; Zhou, et al. Solution-processed antimony selenide heterojunction solar cells. *Adv. Energy Mater*., **2014**, *4*, 1301846.

(26) Södergen, S.; Hagfeldt, A.; Olsson, J.; Lindquist, S.-E. Theoretical models for the action spectrum and the current-voltage characteristics of microporous semiconductor films in photoelectrochemical cells. *J. Phys. Chem.*, **1994**, *98*, 5552.

(27) Laurence, P. "Sticky electrons" transport and interfacial transfer of electrons in the dye-sensitized solar cell. *Acc. Chem. Res*., **2009**, *42*, 1839-1847.

(28) Krbal, M.; Kucharik, J.; Sopha, H.; Nemec, H.; Macak, J. M. Charge transport in anodic TiO_2 nanotubes studied by terahertz spectroscopy. *Phys. Status Solidi RRL* **2016**, *10*, 691-695.

(29) Macak, J. M.; Ghicov, A.; Hahn, R.; Tsuchiya, H.; Schmuki, P. Photoelectrochemical properties of N-doped self-organized titania nanotube layers with different thicknesses. *J. Mater. Res.* **2006**, *21*, 2824-2828.

(30) Macak, J. M. in *Electrochemically engineered nanoporous materials: methods,properties and applications*, Santos, A.; Losic, D.; Eds.; Springer, 1st edn, **2015**, vol. 220, ch. 3, pp. 65.

(31) Ko, B. S.; Sung, S. J.; Kim, D. H.; Lee, D. H.; Hwang, D. K. Effects of annealing on structural and electrical properties of sub-micron thick CIGS films. *Curr. Appl. Phys.*, **2013**, *13*, S135-S139.

(32) Das, S; Zazpe, R.; Prikryl, J.; Knotek, P.; Krbal, M.; Sopha, H.; Podzemna, V.; Macak, J. M. Influence of annealing temperatures on the properties of low aspect-ratio TiO_2 nanotube layers. *Electrochimica Acta*, **2016**, *213***,** 452-459.

(33) Liu, H.; Chang, L. L. Phase relations in systems of tin chalcogenides. *J. Alloys Compd.*, **1992**, *185*, 183-190.

(34) Al-Alamy, F.A.S., Balchin, A. A. The growth by iodine vapour transport and the crystal structures of layer compounds in the series SnS_xSe_{2-x}($0 \leqslant x \leqslant 2$), $Sn_xZr_{1-x}Se_2$ ($0 \leqslant x \leqslant 1$), and TaS_xSe_{2-x} ($0 \leqslant x \leqslant 2$. *J. of Growth and Design*, **1977**, *38*, 221-232.

(35) Whittles, T. J.; Burton, L. A.; Skelton, J. M.; Walsh, A.; Veal, T. D.; Dhanak, V. R. Band alignments, valence bands, and core levels in the tin sulfides SnS, SnS_2, and Sn_2S_3: experiment and theory. *Chem. Mater.*, **2016**, *28*, 3718-3726.

(36) Beranek, R. (Photo)electrochemical methods for the determination of the band edge positions of TiO_2-based nanomaterials. *Adv. Phys. Chem.*, **2011**, 786759.

Table of Contents Graphics